JFM RAPIDS
journals.cambridge.org/rapids

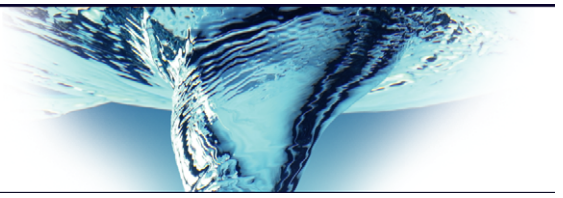

Dynamics of droplet breakup in a T-junction

D. A. Hoang, L. M. Portela, C. R. Kleijn, M. T. Kreutzer† and V. van Steijn

Department of Chemical Engineering, Delft University of Technology, Julianalaan 136, 2628BL, Delft, The Netherlands

(Received 26 October 2012; revised 5 January 2013; accepted 7 January 2013; first published online 7 February 2013)

The breakup of droplets due to creeping motion in a confined microchannel geometry is studied using three-dimensional numerical simulations. Analogously to unconfined droplets, there exist two distinct breakup phases: (i) a quasi-steady droplet deformation driven by the externally applied flow; and (ii) a surface-tension-driven three-dimensional rapid pinching that is independent of the externally applied flow. In the first phase, the droplet relaxes back to its original shape if the externally applied flow stops; if the second phase is reached, the droplet will always break. Also analogously to unconfined droplets, there exist two distinct critical conditions: (i) one that determines whether the droplet reaches the second phase and breaks, or it reaches a steady shape and does not break; and (ii) one that determines when the rapid autonomous pinching starts. We analyse the second phase using stop–flow simulations, which reveal that the mechanism responsible for the autonomous breakup is similar to the end-pinching mechanism for unconfined droplets reported in the literature: the rapid pinching starts when, in the channel mid-plane, the curvature at the neck becomes larger than the curvature everywhere else. The same critical condition is observed in simulations in which we do not stop the flow: the breakup dynamics and the neck thickness corresponding to the crossover of curvatures are similar in both cases. This critical neck thickness depends strongly on the aspect ratio, and, unlike unconfined flows, depends only weakly on the capillary number and the viscosity contrast between the fluids inside and outside the droplet.

Key words: breakup/coalescence, drops and bubbles, micro-/nano-fluid dynamics, microfluidics

1. Introduction

The breakup of droplets in confined geometries, such as found in microfluidic devices with branching networks and in two-fluid flows in porous media, is markedly different from the breakup of droplets in unconfined extensional or straining flows.

† Email address for correspondence: m.t.kreutzer@tudelft.nl

doi:10.1017/jfm.2013.18

Relevant questions are the strength of the flow needed to cause breakup and the mechanism by which this occurs.

The literature on unconfined breakup in Stokes flow dates back to pioneering work by Taylor (1934), who showed that under steady extensional flow, there exists a critical strain rate G below which a droplet of radius a is extended and assumes a steady elongated shape with a length l, and above which the droplet deforms continuously until it breaks. Expressed as a capillary number $Ca = \mu Ga/\gamma$, where γ is the interfacial tension between the fluids, this critical strain rate, to which corresponds a critical droplet length, depends only on the viscosity contrast $\lambda = \hat{\mu}/\mu$ of the fluids inside and outside the droplet. The fate of droplets that are extended at supercritical strain rates was studied in great detail (Stone, Bentley & Leal 1986; Stone & Leal 1989) by stretching droplets and suddenly stopping the flow in a computer-controlled four-roll mill. These experiments revealed that there exists a second critical droplet length, beyond which the droplets break even without an external driving flow, and below which droplets relax back to a sphere. This second critical length, again, depends only on the viscosity contrast λ. In fact, Stone and co-workers' stop–flow experiments revealed many of the relevant and interesting flow features of breaking droplets, such as capillary instabilities similar to the pinching of a cylindrical jet, end-pinching, the formation of satellite droplets, etc., that go far beyond (pseudo-)steady analysis of the maximum strain rate that a droplet can withstand.

A confined geometry that resembles the extensional flows is a T-junction with equal arms into which a long droplet is driven and pushed into both arms. Droplets in the junction then either break up or reach a steady shape; this steady shape might be unstable, in which case the droplet eventually escapes into one of the arms. Link *et al.* (2004) demonstrated that here too, a critical droplet length exists, corresponding to a critical capillary number expressed as $Ca = \mu U/\gamma$, with U the mean velocity flowing into the T-junction. In this confined flow, on dimensional grounds, the ratio of droplet length to channel width $\epsilon = (l/w)$ is relevant, and experiments indeed reveal that the boundary between breakup and non-breakup regimes has the form $Ca = f(\epsilon, \lambda)$. Link *et al.* (2004) used instability arguments similar to jet breakup to predict this transition. More in the spirit of Taylor's analysis, Leshansky & Pismen (2009) predicted the transition by calculating pseudo-steady droplet shapes using a two-dimensional model in which the capillary instability is not operative. Even though their model cannot possibly capture the complex three-dimensional shape of long confined droplets, their theory successfully predicts, up to an $O(1)$ constant, whether droplets break. However, the mechanisms that govern the dynamics beyond the critical capillary number, i.e. for breaking droplets, have remained unclear. Jullien *et al.* (2009) observed that breaking droplets suddenly pinch, which suggests that confined droplets also exhibit a critical shape beyond which breakup is autonomous. Even though, as we will show here, this second critical shape is not generally the same as the critical shape associated with the question of whether a droplet breaks, these shapes are used interchangably in current literature (e.g. Jullien *et al.* 2009; Fu *et al.* 2011). Similarly to unconfined flows, we use stop–flow numerical experiments to clarify this confusion between steady-state features of confined droplets and the three-dimensional surface-tension-driven mechanisms of rapid pinching.

The present paper explores numerically the fate of droplets in a T-junction, exposed to flow rates above the critical value for breakup. We restrict ourselves to the Stokes flow regime; inviscid breakup dynamics are very different (see e.g. Eggers & Villermaux 2008). We shall see that the breakup dynamics of these confined droplets in many ways resembles their unconfined equivalent. Of course, the shape of the

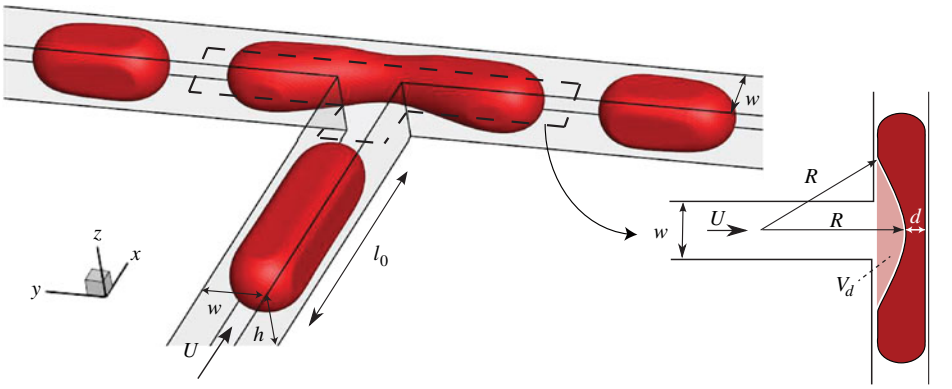

FIGURE 1. Geometry of the problem and top-view of the deforming droplet.

confining channel is now a relevant parameter, in addition to the viscosity contrast and initial droplet size. In simulations, the stop–flow experiments are feasible with little effort, and reveal many interesting aspects that are difficult if not impossible to observe in physical experiments. Similarly in the spirit of Stone *et al.* (1986)'s analysis, we seek to find critical features of the droplet shape that determine when a droplet will break up autonomously even when the flow is stopped abruptly.

2. Problem formulation

Consider the droplet of viscosity $\hat{\mu}$ and density $\hat{\rho}$ in figure 1 that flows from a channel of width w and height h into a T-junction with two equal arms of the same width w and height h. The droplet is too large to remain spherical inside the channel and has a length $l_0 > w$. It is surrounded by an outer fluid of viscosity μ and density ρ, which flows through the feed branch of the T-junction with mean velocity U. We use the fluid properties reported by Link *et al.* (2004) and Jullien *et al.* (2009) as a set of base parameters: for the outer fluid $\mu = 8$ mPa s and $\rho = 770$ g l^{-1}, for the droplet $\hat{\mu} = 1$ mPa s and $\hat{\rho} = 1000$ g l^{-1} and $\gamma = 5$ mN m^{-1}. Velocities in the feed channel of cross-section 30 μm × 30 μm were varied in the range $U = 0.5$–17.5 mm s^{-1}. We varied the viscosity contrast by changing the droplet viscosity, $10^{-3} < \lambda < 10$, and the channel aspect ratio by changing h, $1/3 < h/w < 1$. Droplet sizes $l_0/w = 2.80$, 5.56, 11.1 and ∞ were considered, where $l_0 = \infty$ was simulated by filling both branches with the droplet fluid at the start. Resulting Reynolds numbers $Re = \rho U w/\mu$ and capillary numbers were in the range $10^{-3} < Re < 10^{-1}$ and $10^{-4} < Ca < 10^{-2}$, respectively. We report and analyse all results in dimensionless form, with pressure rescaled with γ/w, time with w/U, and all geometric parameters with w.

Simulations are performed using the finite-volume-based code OpenFOAM-1.6 (Weller *et al.* 1998), in which the fluid interface is represented by the volume-of-fluid (VOF) method. We use hexahedral meshes and refine recursively four times the cells adjacent to the wall to resolve the thin lubrication films surrounding the droplet. At the two exits, we prescribe a reference pressure and zero gradient of the volume fraction. At the walls, we apply the no-slip boundary condition and use an equilibrium contact angle $\theta_e = 0°$. We initialize the simulation with a rectangular droplet, more

than $10w$ upstream of the T-junction, and let the droplet relax to an equilibrium shape. We then start the flow in the feed channel and run it until the two daughter droplets start to leave the computational domain, which happens well after the breakup is complete. We have validated the numerical scheme by reproducing the thickness of the film that lubricates a long bubble in a tube (Bretherton 1961) within 10 % for $Ca = O(10^{-3})$. A second validation was the case of droplet formation at a T-junction as described by van Steijn, Kleijn & Kreutzer (2009), for which experimental data are available on the evolution of the shape of the droplet and the droplet volume after pinch-off for capillary numbers in the same range as those used in the present study ($10^{-4} < Ca < 10^{-2}$). Our numerical code accurately reproduces the evolution of the neck thickness and captures the droplet volumes within 5 %. In these validation studies, as well as in the breakup study presented here, grid-independent results were obtained with 30×30 cells in a square channel cross-section. Details on the numerical methods employed and the validation can be found in Berberovic *et al.* (2009) and Hoang *et al.* (2012).

All published experimental data cited above are only available as the evolution of droplet shapes measured from top-view micrographs and as derived parameters, like the thickness of the neck d and the in-plane radius of curvature R, both shown in figure 1. We further detail the process with time- and space-resolved velocity and pressure fields, which are difficult to obtain experimentally.

3. The mechanism of droplet pinching

3.1. *Breakup of droplets in T-junctions*

We begin by describing the subsequent stages of droplet deformation and flow when a droplet flows into the T-junction. In all cases, the capillary number was well above the critical value for breakup, $Ca = 6 \times 10^{-3}$ for $l_0 = 2.80$, $Ca = 2 \times 10^{-4}$ for $l_0 = 5.56$, similar to $l_0 \approx 0.98 Ca^{-0.21}$ from Leshansky & Pismen (2009). We set $t = 0$ at the moment when the droplet has entirely departed from the feed channel. From this moment on, the driving fluid deforms the droplet in the centre of the T-junction resulting in a dumbbell-like droplet shape as shown in figure 1. The neck connects two half-droplets, which adopt the shape of a semi-infinite droplet in a rectangular channel as described by Wong, Radke & Morris (1995), with a near-flat film surrounding the droplet, except near the corners of the channel where the half-droplets are separated from the wall by a meniscus of radius $r^{-1} \sim 2(1 + h^{-1})$. Flow of the continuous phase around the droplet predominantly occurs through these corner regions, which we call gutters. Early in the breakup, the neck takes the shape of a circular arc with radius R at the mid-plane of the channel ($z/h = 0.5$) as shown in figure 2 for $t = 0.53$. The apparent macroscopic contact angle follows the theory of the hydrodynamics of wetting (Tanner 1979) as proposed by Leshansky *et al.* (2012). Once the neck detaches from the top and bottom wall as shown in the $z/h = 0.1$ plane at $t = 1.12$, the interface no longer assumes a circular arc shape at $z/h = 0.5$. At $t = 1.33$, the local radius of curvature at the neck further decreases until the droplet breaks into two equal daughter drops. Simulations for different droplet sizes show that the flow features are essentially identical in the centre of the T-junction, regardless of the droplet size.

To further our understanding, we turn our attention to the pressure and velocity fields around the neck region as shown in figure 2. At first, fluid from the feed channel spreads out to the gutters and pushes the interface inwards to form a necking region. At $t = 0.53$, the droplet still touches the top and bottom walls in the middle via a thin lubricating film. At $t = 0.67$ (not shown in figure 2), the driving liquid has pushed the

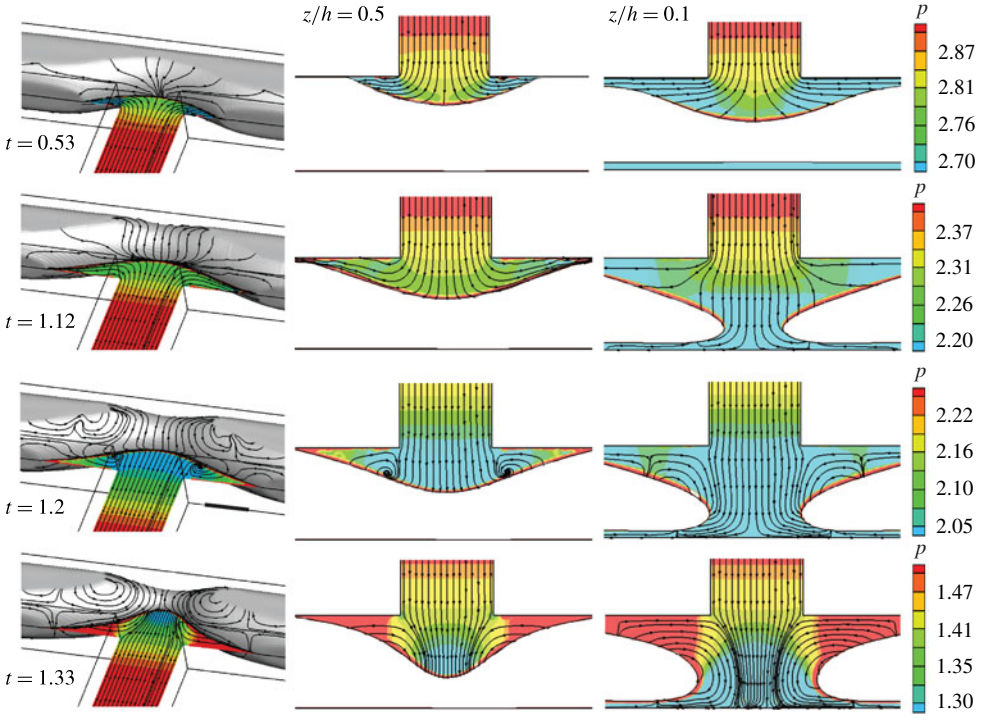

FIGURE 2. Pressure and velocity distribution at four different times during the breakup. $Ca = 6.25 \times 10^{-3}$, $Re = 0.01$, $l_0 = 5.65$, $\lambda = 0.125$, $h = 1$.

neck sufficiently inwards to detach the droplet from the top and bottom walls. From this moment onwards, the fluid also flows through the opening that forms near the top and bottom walls into the gutters opposite the feed channel, as shown for $t = 1.12$; however, the flow in these opposite gutters does not continue to the droplet ends, as can be seen by the stagnation point on the droplet surface. Later, at $t \approx 1.2$, flow to the gutters adjacent to the feed channel ceases. Pressure builds up where the gutters meet the necking region and liquid starts to flow back to the neck, where the pressure is lower. Still later, at $t = 1.33$, a flow to the middle of the T-junction is observed from the entrance of all eight gutters, where the total flow in the gutters adjacent to the inlet is 66 times larger than that in the opposite gutters. A stagnation line is found on the droplet surface in the $|y| \approx 1.2$ plane in both branches. A result of this flow reversal is that the constriction is accelerated, because the incoming fluid can no longer escape.

3.2. *Three-dimensional effects*

A topic of recurring interest has been whether a two-dimensional description of the breakup captures the relevant phenomena. In a two-dimensional analysis, the shape of the lubricating film between the far ends of the breaking droplet and the neck is amenable to a self-similarity analysis, as is the flow through it. Recall that two-dimensional-based predictions of whether the droplet breaks up compared favourably with experiments (Leshansky & Pismen 2009; Jullien *et al.* 2009). As the two-dimensional lubricating film is thin, flow through it is minimal, and the droplet

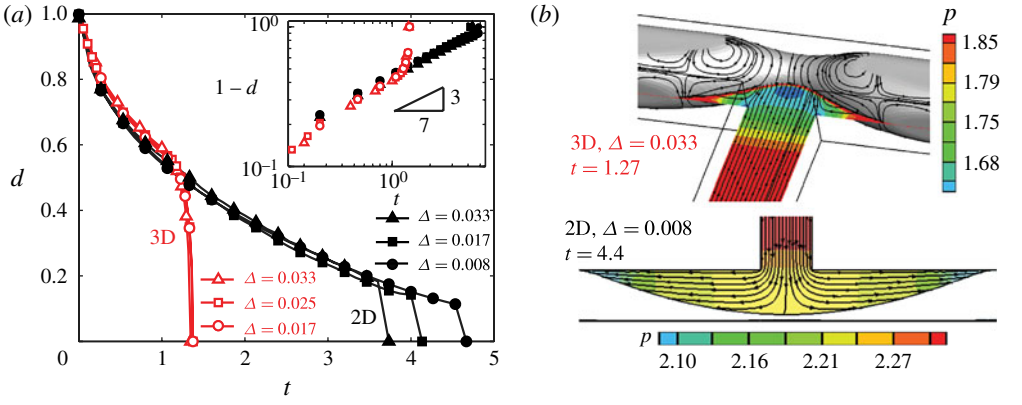

FIGURE 3. (*a*) Evolution of the neck thickness in three-dimensional (red-open symbols) and two-dimensional (black-closed symbols) for different grid resolutions Δ ($h = 1$, $\lambda = 0.125$, $l_0 = 5.56$ and $Ca = 6.25 \times 10^{-3}$). Inset: the same data as $\log(1 - d)$ versus $\log(t)$. (*b*) Pressure and velocity field of three- and two-dimensional simulations just before pinch-off.

obstructs flow to the branches. Leshansky *et al.* (2012) used this all-but-complete obstruction to develop a self-similar description for the breakup dynamics based on the notion that, without leakage through the film, the depression volume V_d of outer fluid near the neck increases linearly with time. In this analysis, $(1 - d) \sim t^{3/7}$, leading to a collapse in a finite time.

We performed two-dimensional simulations, equivalent to the full three-dimensional simulations of breakup described above. Figure 3(*a*) shows the evolution of neck thickness for both the two- and three-dimensional simulations. In agreement with Leshansky *et al.* (2012), we find that in two dimensions the thickness of the neck decreases monotonically until a grid-dependent collapse (a consequence of the VOF method, see also Afkhami, Leshansky & Renardy 2011). The 3/7 scaling describes the data well, as shown in the inset. The three-dimensional evolution follows the two-dimensional data very closely until $d \approx 0.5$. In fact, in three dimensions, $d \approx 1 - 0.58\,(0.25/3Ca)^{-1/7}\,t^{3/7}$, as in two dimensions. This agreement demonstrates that in the early stages of breakup, flow past the semi-obstructing ends is similar in two and three dimensions, with negligible influence of the Laplace pressure due to the out-of-plane curvature, $p \sim d^{-1}$, on the droplet surface at the neck. This, and the small influence of the flow through the gutters, explains why the two-dimensional theory to predict whether a droplet breaks works well in three dimensions: as is the case for unconfined flows, the maximum steady-state droplet deformation is moderate, with, in fact, $d \approx 0.5$ as the maximum deformation (Leshansky & Pismen 2009).

Three-dimensional capillary effects significantly influence the breakup dynamics for $d < 0.5$. In three dimensions, the grid-independent accelerated pinch-off happens well before the two-dimensional breakup. The neck starts to collapse at $d \approx 0.5$, initiating a very fast second phase, resulting in a breakup at $t = 1.37$, much faster than the two-dimensional value of $t = 3.54\,(0.25/3Ca)^{1/3} = 8.39$ (Leshansky *et al.* 2012). As a result, the depression volume $V_d \sim t$ remains small and the range of droplet lengths for which a 'tunnel' opens during the breakup (the 'non-obstructed' regime) is smaller than predicted for two dimensions. The evolution of $d(t)$ with tunnel opening

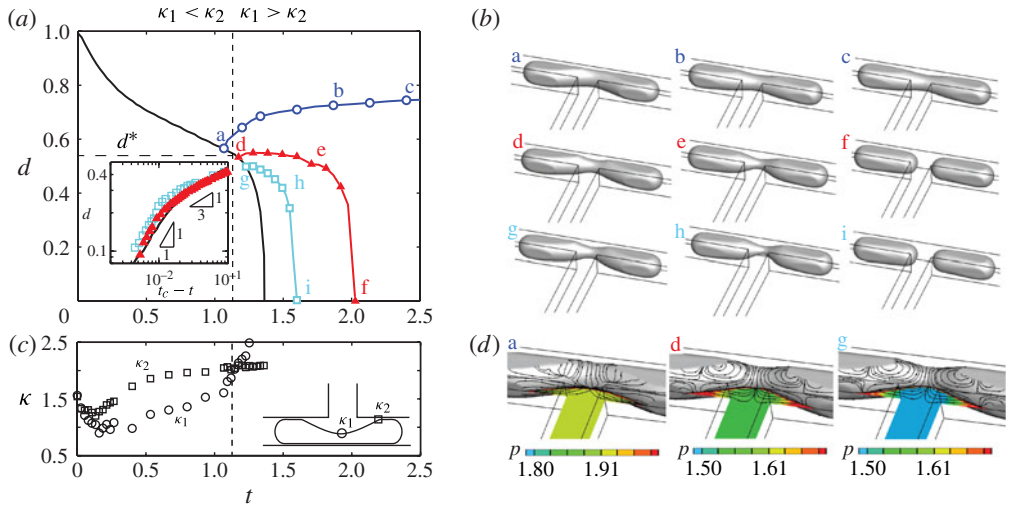

FIGURE 4. (*a*) Evolution of the neck thickness in continuous (solid black line) and stop–flow simulations (coloured symbols). Inset: $\log d$ versus $\log(t_c - t)$. (*b*) Droplet shapes in stop–flow simulations, corresponding to (*a*). (*c*) Evolution of the curvature at indicated locations in the continuous simulation. (*d*) Pressure and velocity field immediately after the start of the stop–flow simulations. (Parameters as in figure 3*a*.)

($l_0 = 2.80$) was identical to that without tunnel opening ($l_0 = 5.56$). More importantly, the smaller breakup time can be compared to the time it takes a droplet to move, partially or entirely, into either branch because of slight imperfections of the symmetry of T-junctions in experiments. The shorter breakup time in three dimensions results, for a given device, in less asymmetry in the volume of the daughter droplets than would be predicted from two-dimensional theory (e.g. Bedram & Moosavi 2011).

Figure 3(*b*) shows when the two- and three-dimensional dynamics diverge prior to pinch-off. In three dimensions, the effect of curvature on the pressure field leads to back flow, whereas in the two-dimensional simulation flow towards the two exits of the T-junction persists until breakup, even though that flow is small. For the case considered here with $h = 1$, the critical value of the neck thickness at the onset of the rapid collapse agrees well with the critical value $d = 1/2$ for a continuous steady-state deformation as calculated by Leshansky & Pismen (2009). As we will discuss below, this result is not generic. In fact, as in unconfined flow (Stone *et al.* 1986, figure 12), there exist two different critical values: (i) one that determines whether the droplet deforms continuously, eventually leading to breakup; and (ii) one that determines the onset of the rapid collapse. Before we discuss features of this second critical neck thickness, we first show how it can be determined from stop–flow simulations.

3.3. *Stop–flow simulations*

We now seek the critical features of the droplet shape that determine whether a droplet will breakup autonomously when the flow is stopped abruptly. As it turns out, the corresponding neck thickness is the same as the critical neck thickness at the onset of rapid collapse. Our starting point is a continuous simulation of droplet breakup (black line in figure 4*a*). In the stop–flow simulations, we extract the shape of the continuous

simulation at different instances and then set the velocity everywhere in the domain equal to zero, keeping the pressure at the outlet constant throughout. We then restart the simulation, which now describes the flow driven by capillary effects alone.

In a first simulation, stopped at $t = 1.07$, the droplet relaxes back to the original shape (circles, blue line in figure 4*a* and the droplet shapes (a–c) in figure 4*b*). Without the driving fluid coming into the T-junction, this process is dominated by the slow flow through the gutters and the droplet reaches its relaxed shape only at $t \gg 1$. The situation is markedly different for a second simulation, stopped at $t = 1.17$ (triangles, red line, shapes (d–f)), where the neck first increases slightly, followed by a gradual decrease and a rapid collapse. In a third simulation, stopped at $t = 1.23$, this initial increase is absent (squares, light blue line, shapes (g–i)), but the final rate $\partial d/\partial t$ of the rapid collapse is similar and equals the rate of the final collapse in the case when the flow is not stopped. The neck scales with $(t_c - t)^{\alpha}$, where t_c is the pinch-off time, with an exponent α which changes from $\alpha \approx 1/3$ at $d = 0.3$ to $\alpha \approx 1$ at $d = 0.1$, which was smallest neck size that we could resolve on our grid, indicating that a (inertial–) viscous–capillary balance is operative in the final stages (Eggers & Villermaux 2008). Figure 4(*d*) shows that stagnation lines on the interface immediately appear for the two stop–flow simulations that lead to breakup, in contrast to the simulation that relaxes back to a single droplet. This highlights the importance of the flow of the outer fluid for the rapid pinch in the centre.

The three stop–flow simulations, taken together, show that once the neck thins beyond a critical value (here, $d^* = 0.53$ at $t = 1.1$), droplet breakup is inevitable. This transition between relaxation and breakup coincides with the start of the rapid collapse for the simulation in which the flow persists, as marked by the point of departure from the line $(1 - d) \sim t^{3/7}$ in the inset of figure 3(*a*). Similarly to droplets that break without further external strain in unconfined flows (Stone *et al.* 1986), confined droplets break due to a surface-tension-driven mechanism. Following Stone *et al.*'s analysis of the droplet shape after stopping the flow, we note that droplets relax when, in the channel mid-plane, the local curvature at the neck, κ_1, is smaller than the curvature everywhere else, such that the surrounding liquid flows away from the neck. By contrast, droplets break when the curvature at the neck is larger than the curvature everywhere else. The comparison between κ_1 and the curvature κ_2 at the entrance of the gutter shows that, indeed, $\kappa_1 - \kappa_2$ reverses sign at the transition between breaking and non-breaking drops (figure 4*c*). The only difference between Stone *et al.*'s analysis and ours is that the location of the maximum curvature is off-centre for unconfined droplets, such that they break into at least three fragments. In fact, the confining geometry prevents the formation of the large bulbous ends, and the inflow at the centre forces the pinch in the middle. Despite this slight difference, our work clearly shows that it is the shape of the droplet alone that drives the pinching: the breakup mechanism is similar to the end-pinching mechanism proposed by Stone *et al.* (1986) for unconfined droplets.

4. Critical shape for autonomous pinching

We now explore how the critical shape for autonomous breakup d^*, which coincides with the point of departure from two-dimensional-like behaviour, depends on the confining geometry. Simulations (continuous and stop–flow) in channels with height-to-width ratios between 1/3 and 1 show the dependence of d^* on h as evident from a comparison of the evolution of the neck thickness in figure 5(*a*). A reduction in h reduces d^*, postponing the onset of the rapid collapse t^*. We note that both d^*

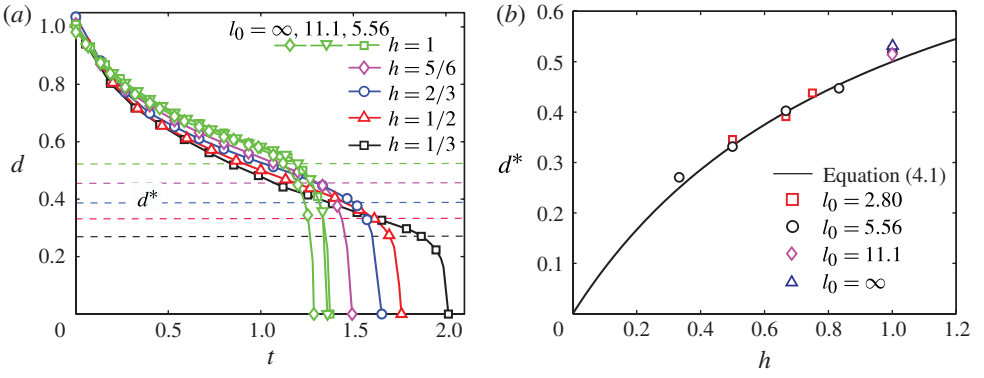

FIGURE 5. (*a*) Evolution of the neck thickness in T-junctions with different height-to-width ratios h ($l_0 = 5.56, 11.1$ and ∞, $Ca = 6.25 \times 10^{-3}$). (*b*) Critical neck thickness d^* versus h. ($l_0 = 5.56, 11.1$ and ∞, $Ca = 6.25 \times 10^{-3}$) and ($l_0 = 2.80$, $Ca = 0.01$).

and $d(t)$ are rather insensitive to droplet length. More quantitatively, we found that all data ($0.33 < h < 1$ and $l_0 \geqslant 2.80$) follow the simple relation

$$d^* = \frac{h}{h+1} \tag{4.1}$$

as shown in figure 5(*b*). This relation was previously developed for the rapid collapse of the neck of droplets forming in T-junctions (van Steijn *et al.* 2009) suggesting that similar mechanisms are at play.

Unlike unconfined droplets, the shape of the droplet at $t = t^*$ is almost independent of the viscosity contrast and the capillary number. Consequently, we expect d^* to be insensitive to both these parameters. Indeed, a comparison of the neck evolution in channels with $h = 1$ shows that d^* only slightly depends on Ca (inset of figure 6*a*), with a decrease in d^* of 15 % over the two orders of magnitude increase of Ca ($9 \times 10^{-4} < Ca < 2.8 \times 10^{-2}$). These results are in line with the experimental observations by Jullien *et al.* (2009) and Fu *et al.* (2011). To study the influence of the viscosity contrast, we varied the viscosity of the droplet $\hat{\mu}$ while keeping the viscosity of the surrounding fluid μ constant. Figure 6(*b*) shows that the onset of rapid pinching does not change with λ. The rate of the pinching decreases with increasing λ, and the exponent in $d \sim (t_c - t)^\alpha$ tends to $\alpha = 1$. One would expect asymmetry in the pinching for two viscous fluids (Eggers & Villermaux 2008), but for the neck sizes that we could resolve we did not observe that (Papageorgiou 1995; Eggers & Villermaux 2008). Due to the higher droplet viscosity, the pinching time increases, by a factor 1.4 going from $\lambda = 0.001$ to $\lambda = 1$ and by a factor 2.4 by going from $\lambda = 1$ to $\lambda = 10$.

We now return to the discussion on the two critical shapes in the breakup of confined droplets. By calculating steady-state shapes without regarding dynamics, Leshansky & Pismen (2009) showed that the first critical droplet shape, which determines whether a droplet breaks, has a neck thickness $d = 0.5$. Even though the second critical droplet shape, beyond which the droplets break autonomously at supercritical velocities, roughly coincides with the first at $h = 1$, this result is

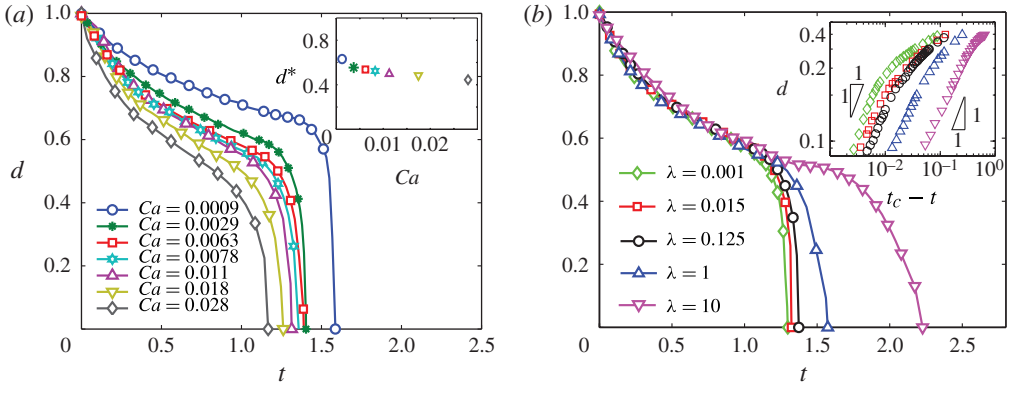

FIGURE 6. (*a*) Influence of the capillary number $9 \times 10^{-4} < Ca < 2.8 \times 10^{-2}$ on the evolution of the neck thickness. Inset: d^* versus Ca ($h = 1$, $l_0 = 5.65$, $\lambda = 0.125$). (*b*) Influence of the viscosity contrast $0.001 < \lambda < 10$ on the evolution of the neck thickness ($h = 1$, $l_0 = 5.65$, $Ca = 6.25 \times 10^{-3}$). Inset: $\log d$ versus $\log(t_c - t)$.

certainly not general. Our simulations show that the second critical drop shape, though insensitive to Ca and λ, strongly depends on the aspect ratio of the channel h.

5. Concluding remarks

We have presented a numerical study on the breakup of droplets confined in a T-junction using full simulations and stop–flow simulations. While stop–flow experiments are notoriously difficult to perform in microfluidic devices, numerical experiments are easily done. Our simulations reveal that the breakup mechanism shows similarities with the breakup of unconfined droplets. The breakup process comprises two distinct phases: in the first phase the droplet goes through a quasi-steady deformation, driven by the externally applied flow, while in the second phase a surface-tension-driven three-dimensional rapid autonomous pinching occurs that is independent of the externally applied flow. The rapid autonomous pinching starts when, in the channel mid-plane, the curvature at the neck rises above the curvature everywhere else. The onset of this pinching depends strongly on the aspect ratio of the confining channel; however, unlike unconfined droplets, it depends only slightly on Ca and λ. This can be understood from the fact that the rapid autonomous pinching is solely driven by the shape of the droplet, which strongly depends on the aspect ratio of the channel, but, contrary to unconfined flows, hardly depends on Ca and λ.

It is important to note that all droplets studied in this work break if we do not stop the flow, i.e. we study the dynamics of droplets at supercritical velocities both in the 'obstructed' and 'non-obstructed' regime. The critical shape characterized by d^* corresponds to the onset of the rapid collapse; it does not correspond to the critical shape associated with the question of whether the droplets break, as addressed by Link *et al.* (2004) and Leshansky & Pismen (2009). Our work reveals that the two critical values for the neck thickness only closely match in channels with an aspect ratio $h = 1$ and it clarifies why these two should not be used interchangably for $h \neq 1$.

Acknowledgement

The authors gratefully acknowledge the financial support from STW and IROP-OSPT, The Netherlands.

References

AFKHAMI, S., LESHANSKY, A. M. & RENARDY, Y. 2011 Numerical investigation of elongated drops in a microfluidic t-junction. *Phys. Fluids* **23** (2), 022002.

BEDRAM, A. & MOOSAVI, A. 2011 Droplet breakup in an asymmetric microfluidic T junction. *Eur. Phys. J.* E **34** (8), 78.

BERBEROVIC, E., VAN HINSBERG, N. P., JAKIRLIĆ, S., ROISMAN, I. V. & TROPEA, C. 2009 Drop impact onto a liquid layer of finite thickness: dynamics of the cavity evolution. *Phys. Rev.* E **79** (3), 036306.

BRETHERTON, F. P. 1961 The motion of long bubbles in tubes. *J. Fluid Mech.* **10** (2), 166–188.

EGGERS, J. & VILLERMAUX, E. 2008 Physics of liquid jets. *Rep. Prog. Phys.* **71** (3), 036601.

FU, T., MA, Y., FUNFSCHILLING, D. & LI, H. Z. 2011 Dynamics of bubble breakup in a microfluidic T-junction divergence. *Chem. Engng Sci.* **66** (18), 4184–4195.

HOANG, D. A., VAN STEIJN, V., PORTELA, L. M., KREUTZER, M. T. & KLEIJN, C. R. 2012 Modelling of low-capillary number segmented flows in microchannels using openfoam. *AIP Conference Proceedings* **1479** (1), 86–89.

JULLIEN, M. C., CHING, M. J. T. M., COHEN, C., MENETRIER, L. & TABELING, P. 2009 Droplet breakup in microfluidic T-junctions at small capillary numbers. *Phys. Fluids* **21** (7), 072001.

LESHANSKY, A. M., AFKHAMI, S., JULLIEN, M.-C. & TABELING, P. 2012 Obstructed breakup of slender drops in a microfluidic T junction. *Phys. Rev. Lett.* **108**, 264502.

LESHANSKY, A. M. & PISMEN, L. M. 2009 Breakup of drops in a microfluidic T junction. *Phys. Fluids* **21** (2), 023303.

LINK, D. R., ANNA, S. L., WEITZ, D. A. & STONE, H. A. 2004 Geometrically mediated breakup of drops in microfluidic devices. *Phys. Rev. Lett.* **92** (5), 054503.

PAPAGEORGIOU, D. T. 1995 On the breakup of viscous liquid threads. *Phys. Fluids* **7** (7), 1529–1544.

VAN STEIJN, V., KLEIJN, C. R. & KREUTZER, M. T. 2009 Flows around confined bubbles and their importance in triggering pinch-off. *Phys. Rev. Lett.* **103**, 214501.

STONE, H. A., BENTLEY, B. J. & LEAL, L. G. 1986 An experimental study of transient effects in the breakup of viscous drops. *J. Fluid Mech.* **173**, 131–158.

STONE, H. A. & LEAL, L. G. 1989 Relaxation and breakup of an initially extended drop in an otherwise quiescent fluid. *J. Fluid Mech.* **198**, 399–427.

TANNER, L. H. 1979 The spreading of silicone oil drops on horizontal surfaces. *J. Phys. D: Appl. Phys.* **12** (9), 1473.

TAYLOR, G. I. 1934 The formation of emulsions in definable fields of flow. *Proc. R. Soc. Lond.* A **146** (858), 0501–0523.

WELLER, H. G., TABOR, G., JASAK, H. & FUREBY, C. 1998 A tensorial approach to computational continuum mechanics using object-oriented techniques. *Comput. Phys.* **12** (6), 620–631.

WONG, H., RADKE, C. J. & MORRIS, S. 1995 The motion of long bubbles in polygonal capillaries. Part 1. Thin films. *J. Fluid Mech.* **292**, 71–94.